N-53795

[redacted]

INVESTIGATION OF THE EFFECTS OF [illegible] BY DISCRETE [illegible] ON THE TOTAL-PRESSURE DISTORTIONS THROUGH SINGLE-STAGE SUBSONIC AXIAL-FLOW COMPRESSORS

by

George C. Ashby, Jr.

Thesis submitted to the Graduate Faculty of the

Virginia Polytechnic Institute

in candidacy for the degree of

MASTER OF SCIENCE

in

Aeronautical Engineering

May 1971

APR 1971
RECEIVED
NASA STI FACILITY
INPUT BRANCH

N71-72206
(ACCESSION NUMBER)
53
(PAGES)
TMX-67011
(NASA CR OR TMX OR AD NUMBER)
FACILITY FORM 602
(THRU)
None
(CODE)
(CATEGORY)

[redacted]

INVESTIGATION OF THE EFFECT OF VELOCITY DIAGRAM PARAMETERS ON INLET TOTAL-PRESSURE DISTORTIONS THROUGH SINGLE-STAGE SUBSONIC AXIAL-FLOW COMPRESSORS

by

George C. Ashby, Jr.

Thesis submitted to the Graduate Faculty of the

Virginia Polytechnic Institute

in candidacy for the degree of

MASTER OF SCIENCE

in

Aeronautical Engineering

APPROVED:

Director of Graduate Studies

Dean of Engineering

APPROVED:

Head of Department

Major Professor

May 1957

Blacksburg, Virginia

[redacted]

TABLE OF CONTENTS

		PAGE
I.	LIST OF FIGURES	3
II.	INTRODUCTION	4
III.	SYMBOLS	8
IV.	ANALYSIS	10
V.	EXPERIMENTAL TESTS	21
	Apparatus	21
	Instrumentation	25
	Test Program and Procedure	30
	Presentation of Data	31
VI.	RESULTS AND DISCUSSION	33
VII.	CONCLUSIONS	41
VIII.	SUMMARY	44
IX.	ACKNOWLEDGMENTS	46
X.	BIBLIOGRAPHY	47
XI.	VITA	48
XII.	APPENDIX	49

I. LIST OF FIGURES

FIGURE		PAGE
1.	Compressor Rotor Velocity Diagram	11
2.	Superposition of Distorted Flow Velocity Diagram on Undistorted Flow Velocity Diagram	12
3.	Velocity Diagrams Analysed	14
4.	Schematic Diagram of Test Compressor Showing Blade Rows and Instrumentation Positions	22
5.	Rotor Used in Investigation	24
6.	Sketch Showing Instrumentation at Each Measuring Station	26
7.	Details of Prism-Type Probe	27
8.	26-Tube Total-Pressure Rake Used to Measure Rod Wake at Station 1	28
9.	25-Tube Shielded Total-Pressure Rake Used to Measure Rod Wake at Station 2	29
10.	Comparison of Measured and Estimated Downstream Rod Wakes With the Measured Upstream Wake for Five Test Configurations at Approximately Design Angle of Attack	34
11.	Comparison of Measured and Estimated Downstream Rod Wakes With Measured Upstream Wake for Rotor Alone; $\xi = \xi_d$, Configuration at Three Angles of Attack	36
12.	Comparison of the Streamline Paths of the Undistorted and Distorted Flows in the Blade Passage	40

[redacted]

II. INTRODUCTION

One of the most important problems associated with high-speed gas-turbine powered aircraft is reduced compressor, and therefore engine, performance resulting from nonuniform distributions of total pressure at the compressor entrance, hereinafter referred to as inlet total-pressure distortions. This inlet total-pressure distortion can affect compressor performance in several ways. It may result in premature surge and therefore reduced engine acceleration margin and altitude operating limits, it may result in rotating stall, in increased compressor-blade vibratory stresses, and/or in reduced engine mass flow (refs. 1, 2, and 3).

The term "inlet" usually refers to the air intake and its diffuser; however, distortions which develop in the ducting from the diffuser exit to the compressor entrance are also classified as inlet distortions. An inlet is designed primarily to accommodate the mass flow required by the engine when the aircraft is flown at its design flight speed and altitude. It is also designed to provide the mass-flow requirements over as large a range of flight conditions as possible. When the aircraft is operated in the vicinity of its design-flight conditions the flow distortions which develop in the inlet are usually small enough to be tolerated. However, operation of the engine at off-design conditions or the aircraft at large angles of attack (or yaw) may result in large inlet flow distortions.

Flow distortions can have several causes and are somewhat dependent on flight speed (ref. 4). At subsonic speeds when the engine is operated at off-design conditions or when the aircraft is flown at high angles of attack or yaw a distorted flow may result because of flow separation from the inlet lip. At supersonic speeds with either the off-design or high angle-of-attack condition, a distorted flow may result because of non-uniform compression at the inlet throat. The diffuser and the ducting from the diffuser to the compressor entrance can also be sources of distortions. Their design is dependent on the internal design of the aircraft and often has to be compromised to avoid interference with the pilot's compartment, structural members, and/or auxiliary equipment. If the flow is diffused or turned too rapidly, flow distortions result due to flow separation from the walls.

Several investigations have been conducted to determine the effects of inlet total-pressure distortion on the performance of specific engines (e.g., refs. 2, 5, and 6). In reference 7 a distortion factor which is a function of the circumferential extents of the distorted and undistorted flow regions and the magnitude of the distortion is correlated with a blade stall function. These studies indicate in general what engine performance penalties are expected with a distortion of given magnitude and extent but do not provide a solution to the problem.

In fact, up to the present time, the only approach to the solution of the problem has been that of reducing the distortion before it

reaches the compressor. References 1 and 2 show that internal boundary-layer bleed at the inlet throat will reduce the total-pressure distortions. They also show that the distortions may be reduced before they reach the compressor entrance when better mixing is provided in the inlet ducting by increasing the diffuser length, by contracting the exit of the diffuser, or by using screens or freely rotating fans. However, since these methods do not completely eliminate the distortion and result in weight, volume, and pressure-recovery penalties, other means of reducing the distortion need to be found.

Investigations of the effect of inlet total-pressure distortions on the performance of specific engines (refs. 2, 5, and 6) show that some distortions were eliminated within the compressor and those which persisted through the whole engine were greatly reduced. These results indicate that some compressor designs may be more effective in reducing an inlet total-pressure distortion than others. If the criterion can be found for designing compressors which will efficiently eliminate inlet total-pressure distortions within the first few stages, the weight, volume, and pressure-recovery penalties which accompany the previously mentioned methods of reducing the distortion before it reaches the compressor need not be endured.

The end result of a compressor stage design are the velocity diagrams at the design radii. When the flow entering a compressor stage has a region of low total pressure and therefore low velocity, the velocity diagrams in this region will not be the same as design.

A comparison of velocity diagrams where only the entering velocity was varied shows that the rotor raises the total pressure of the low velocity flow more than it does the total pressure of the high velocity flow; therefore, in general, an inlet total-pressure distortion will be reduced across a rotor. The purpose of the present investigation is to determine the velocity diagram which is most effective in reducing inlet total-pressure distortions. The results of this investigation were verified by the introduction of a small disturbance (rod wake) upstream of a compressor stage.

III. SYMBOLS

c_p	specific heat of air at constant pressure, ft-lb/slug-^oR
c_v	specific heat of air at constant volume, ft-lb/slug-^oR
H	total enthalpy, $\left(u + \frac{p}{\rho}\right)$ ft-lb/slug
u	internal energy, ft-lb/slug
p	static pressure, lb/sq ft
P	total pressure, lb/sq ft
dP	total-pressure difference between the undistorted flow and point in distorted flow, lb/sq ft
q	dynamic pressure, $\frac{1}{2}\rho V^2$, lb/sq ft
R	perfect-gas constant, ft-lb/slug-^oR
t	static temperature, ^oR
U	blade speed, ft/sec
V	velocity, ft/sec
ΔV_t	change in tangential velocity across rotor, ft/sec
φ	flow coefficient, $\frac{V_a}{U}$
α	angle of attack relative to blade chord, $\beta_{1R} - \xi$, deg
β	flow angle measured from axis of rotation, deg
θ	turning angle, $\beta_{1R} - \beta_{2R}$, deg
ξ	blade-setting angle (angle between blade chord and axis of rotation), deg
ρ	air density, slugs/cu ft

Subscripts:

1	upstream of guide vane
1	upstream of rotor
2	downstream of rotor
a	axial direction
d	design condition
R	relative coordinates
t	tangential direction

IV. ANALYSIS

A compressor rotor velocity diagram at a given radius is shown in Figure 1. The flow enters the blade row axially on absolute coordinates with a velocity V_1. Relative to the blades, the entering velocity and air inlet angle are V_{1R} and β_{1R}, respectively. The flow is turned in the blade passage and exits the blades on relative coordinates with a velocity V_{2R} at an angle of β_{2R}. On absolute coordinates, the flow has an exit velocity and direction of V_2 and β_2, respectively.

An inlet total-pressure distortion can have its variation in the radial or circumferential direction. The ensuing discussion considers circumferential distortions in the flow at a given blade element without regard to the influence of the flow at other blade elements. Figure 2 shows the circumferential velocity profile, at a given radius, of a flow with a distortion entering a compressor rotor-blade row. Although the angle of attack relative to the blade would not instantaneously become that associated with each velocity vector of the distorted region as the blade passes through the distortion, for the purpose of our analysis the assumption that it does will be sufficient. This assumption allows the velocity diagram associated with a point in the distorted region (dashed lines) to be superimposed on the velocity diagram for any point in the undistorted region (solid lines), as shown in Figure 2. This superposition method is used in the analysis of the three representative inlet-stage velocity diagrams shown in

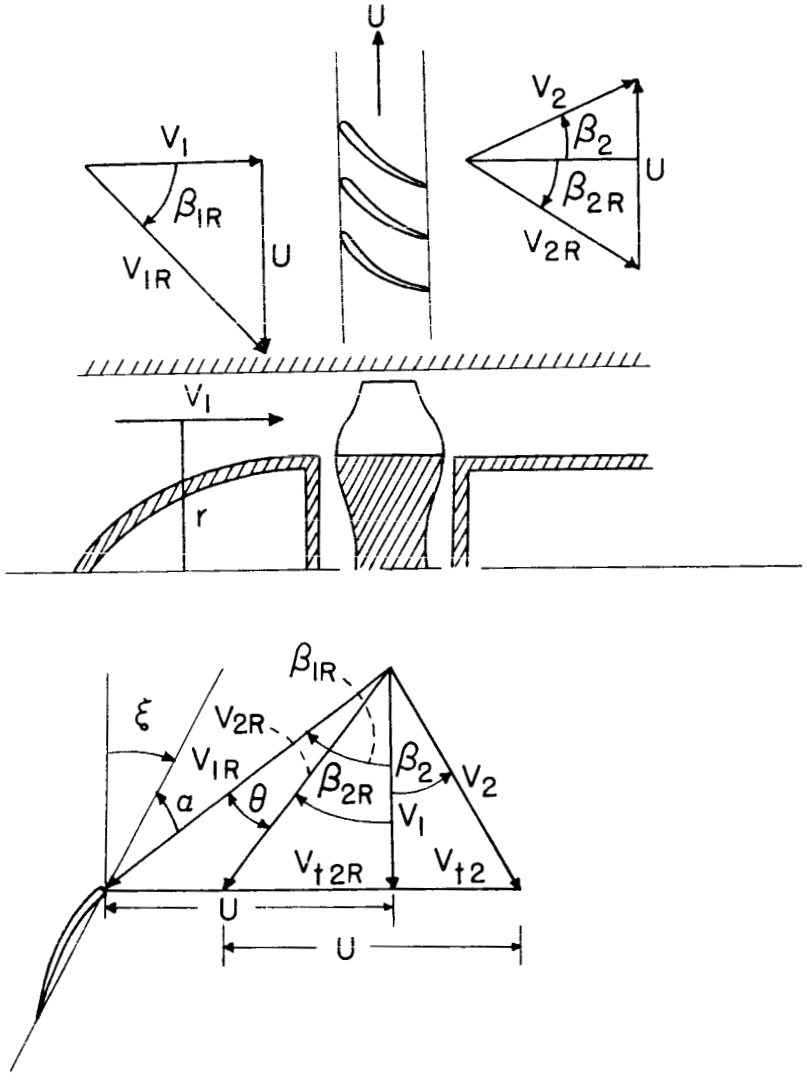

Figure 1.- Compressor rotor velocity diagram.

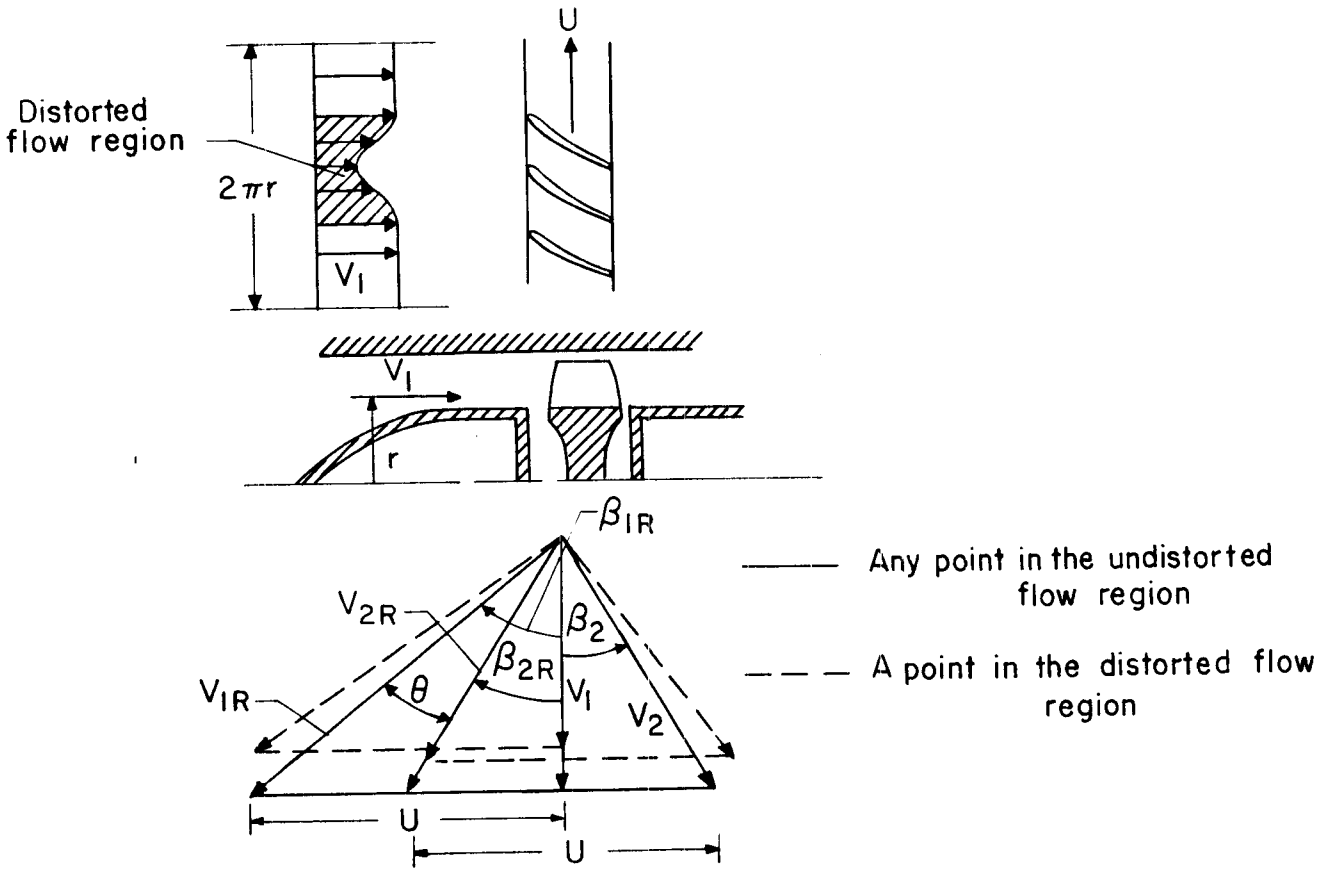

Figure 2.- Superposition of distorted flow velocity diagram on undistorted flow velocity diagram.

Figure 3. The analysis was made on the basis of incompressible flow with the following assumptions:

1. The undistorted and distorted flows enter the rotor with the same absolute direction.

2. The static pressure of the distorted and undistorted flow is equal at the inlet and also at the exit of the rotor.

3. The increase of blade angle of attack in the distorted flow is not sufficient to cause blade stall.

4. The distorted flow is turned in the rotor passage to the same exit direction, relative to the rotor, as the undistorted flow $\left(\frac{d\theta}{d\alpha} = 1.0\right)$.

Figure 3(a) is the velocity diagram of a rotor alone with an undistorted-flow inlet-air angle of 45° (β_{1R}). Both the distorted and undistorted flows enter the rotor axially. Since the blade speed is constant, the extremities of the inlet relative-velocity vectors of the two flows lie along a line parallel to the inlet absolute-velocity vectors. The inlet relative-velocity vector of the distorted flow, compared with that of the undistorted flow, has a smaller magnitude, produces a larger inlet-air angle (β_{1R}), and therefore a greater angle of attack ($\beta_{1R} - \xi$) to the rotor blade. Under assumption 4, the two flows exit relative to the rotor in the same direction. The equality of static pressure (assumption 2) and the difference in magnitude between the inlet relative velocities require that the magnitude of the exit relative velocity be less for the distorted flow. Because

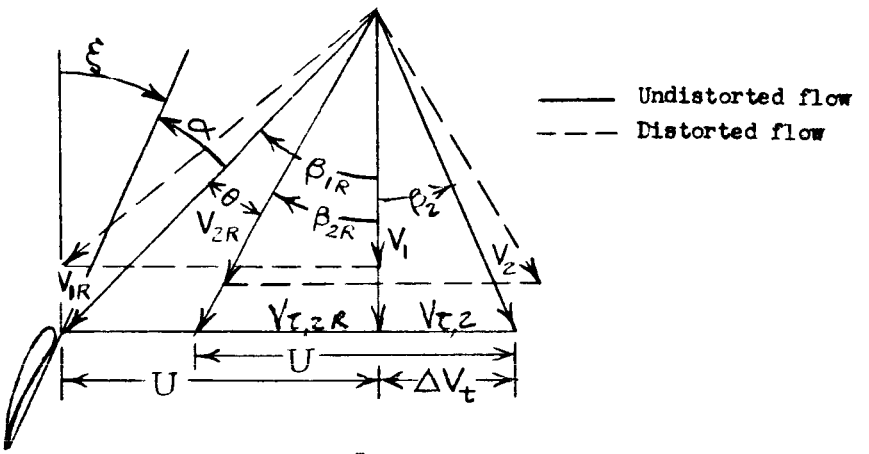

(a) Rotor alone, $\beta_{1R} = 45^\circ$ in undistorted flow.

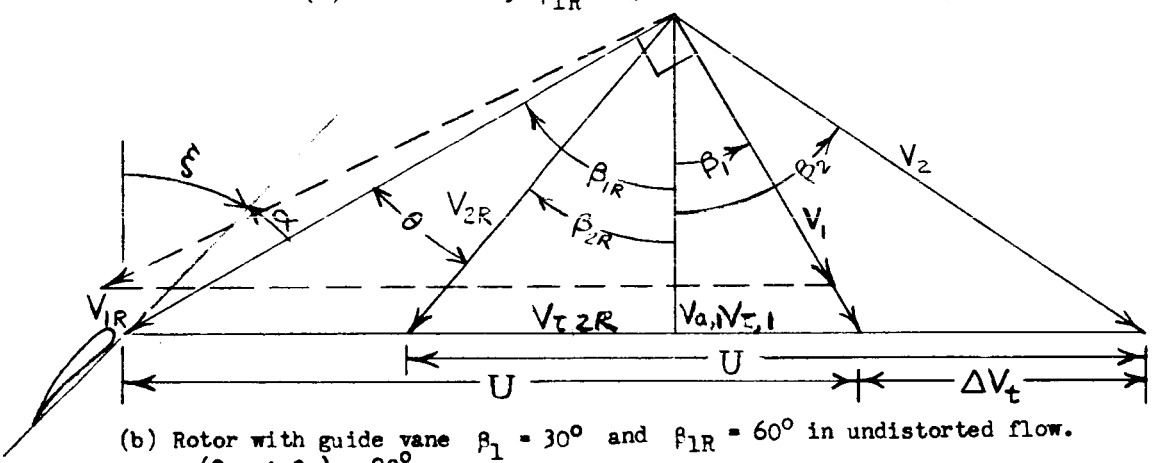

(b) Rotor with guide vane $\beta_1 = 30^\circ$ and $\beta_{1R} = 60^\circ$ in undistorted flow. $(\beta_{1R} + \beta_1) = 90^\circ$.

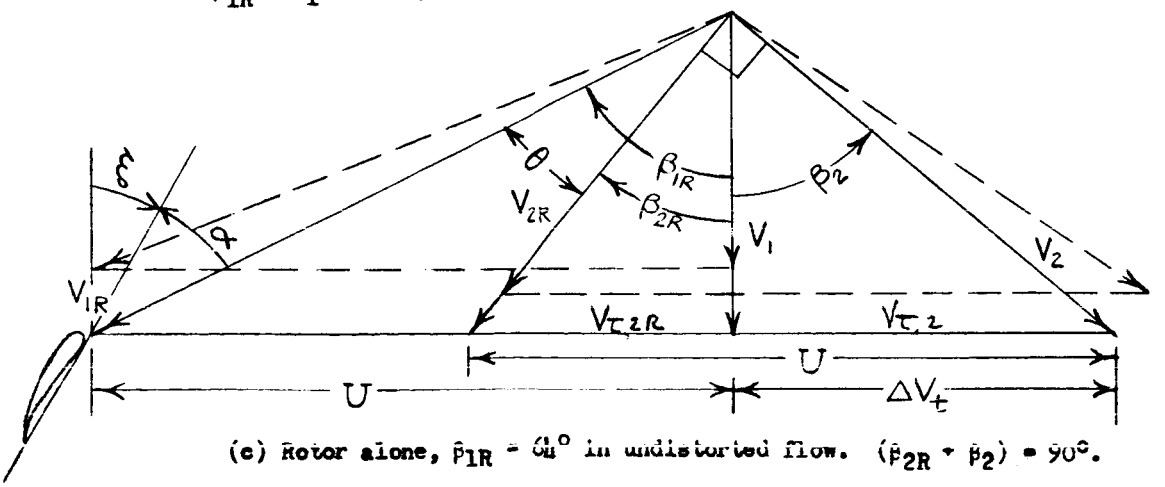

(c) Rotor alone, $\beta_{1R} = 60^\circ$ in undistorted flow. $(\beta_{2R} + \beta_2) = 90^\circ$.

Figure 3.- Velocity diagrams analyzed.

the static pressures are equal, the difference in total pressure between the two flow regions on absolute coordinates is proportional to the differences between the squares of their absolute velocities. For this diagram (Figure 3(a)), the distortion has been reduced approximately 50 percent by the rotor.

Figure 3(b) is the velocity diagram of a guide-vane-rotor combination. The guide vane turns the flow 30° in the direction of rotor rotation and the rotational velocity is such that the undistorted-flow inlet-air angle to the rotor (β_{1R}) is 60°. Since the included angle between the inlet flow directions on the absolute and relative frames of reference is 90° ($\beta_{1R} + \beta_1 = 90°$), the inlet relative-velocity vector of the undistorted flow is perpendicular to the line along which lie the extremities of the inlet relative-flow vectors (V_{1R}) of both flows. Therefore, the inlet relative-flow vectors of both flows will be approximately the same length for distortions which do not produce a large change in the relative inlet-air angle. A change of 8° in the inlet-air angle, due to a distortion, will result in a difference in relative velocity of 1 percent. The static pressures of these two streams are equal; therefore, the total pressures relative to the rotor are equal. Both flows are turned to the same relative exit direction and, because of the required equality of static pressure, the vectors are coincident. Since the rotational speed is constant the vectors are also coincident in the absolute frame of reference, and, therefore, the exit total pressures are the same. For this diagram, under the

assumptions made, the distortion would be eliminated by the first stage. It is noted that a significant parameter for the elimination of the distortion in the first stage of a compressor is the included angle between the relative and absolute flow directions entering the rotor.

An included angle of 90° between the relative and absolute flow directions is also significant when it occurs at the exit of the rotor (as evidenced by Figure 3(c)). This velocity diagram is for a rotor alone with an undistorted-flow inlet-air angle (β_{1R}) of 64°. The analysis of the flow entering the rotor for this diagram is the same as that for the diagram of Figure 3(a). The turning angle has been selected so that the angle between the relative and absolute flow directions leaving the rotor is 90° ($\beta_{2R} + \beta_2 = 90°$). Thus, with the same reasoning being used as in Figure 3(b), the absolute velocities in the distorted and in the undistorted flow regions are approximately equal. Because of uniform static pressure for the two flows, the total pressures of the flows are equal. The difference in the absolute flow angle can be rectified by the stator and the distortion will be eliminated by the first stage.

From the velocity diagrams, it can also be seen that the deficit in total pressure between the distorted and undistorted flow is reduced because the distorted flow is energized by the rotor more than is the undistorted flow. This is manifested by the larger change in tangential

velocity across the rotor for the distorted flow. By using the well-known equation for the energy added by the rotor

$$H_2 - H_1 = U_2 V_{t,2} - U_1 V_{t,1} \tag{1}$$

and the assumptions used for the velocity-diagram analysis, the difference between the total pressures of any point in the undistorted flow region and a point in the distorted flow region after passing through the rotor can be expressed in terms of the flow angles. The resulting equation, the derivation of which is given in the appendix, for incompressible flow is

$$dP_2 = dP_1 \left[\cos(\beta_1 + \beta_{1R}) \cos(\beta_2 + \beta_{2R}) \frac{\cos \beta_1}{\cos \beta_{1R}} \frac{\cos \beta_{2R}}{\cos \beta_2} \right] \tag{2}$$

When the upstream total-pressure deficit and the velocity diagram for the undistorted flow are known, the downstream total-pressure deficit can be determined by using this equation.

Equation (2) verifies the analysis of the velocity diagrams. It can be seen that if either or both of the included angles $(\beta_1 + \beta_{1R})$ and $(\beta_2 + \beta_{2R})$ is 90°, the total-pressure deficit between the distorted and undistorted flows will be eliminated. If one of the included angles is greater than 90°, the total-pressure deficit will be negative. The rotor, therefore, more than made up the total pressure needed to raise the distorted-flow total pressure to that of the undistorted flow. It is interesting to note that if both of the included angles are greater

than 90°, the deficit will not be completely eliminated. When the velocity diagram has neither of the included angles equal to 90°, the decrease in the inlet total-pressure distortion across the rotor depends not only on the magnitude of the included angles at the entrance and exit of the rotor but also on the relative magnitude of the absolute and relative flow angles at the entrance and at the exit; that is, the larger the ratios of $\frac{\beta_1}{\beta_{1R}}$ and $\frac{\beta_{2R}}{\beta_2}$, the greater will be the decrease in the distortion for given included angles. The inlet total-pressure distortion could increase across the rotor if the included angles were very small, and if β_1 and β_{2R} were much smaller than β_{1R} and β_2, respectively. The analysis has been given in terms of the flow angles of the velocity diagram. However, the velocity diagram is the end result of a compressor-stage design, and an analysis in terms of the design parameters, flow coefficient (φ), and loading (turning angle) would be of more interest to the designer. Considering the conclusions of the analysis with respect to these parameters, it is found that for an included angle ($\beta_R + \beta$) of 90° the flow coefficient (φ) reaches a maximum of 0.5 when $\beta_R = \beta = 45°$. The flow coefficient would have to be less than 0.5 for an included angle to be greater than 90°. When an included angle is 90°, there is no apparent influence of loading on the amount of distortion elimination since the $\frac{\cos \beta_{2R}}{\cos \beta_2}$ term of equation (2), which increases as loading (turning angle) increases, has no influence. However, for included angles other than 90°, both

the flow coefficient and loading influence the amount of distortion elimination. The entering flow coefficient (φ_1) in conjunction with the guide-vane exit angle (β_1) establishes the entering included angle. The exiting flow coefficient (φ_2) in conjunction with the loading (turning angle) determines the downstream included angle. Since included angles approaching 90° are desired, the flow coefficient should be kept in the vicinity of 0.5. For given values of flow coefficients, since β_1 and loading (turning angle) establish the values of the $\frac{\cos \beta_1}{\cos \beta_{1R}}$ and $\frac{\cos \beta_{2R}}{\cos \beta_2}$ terms, respectively, of equation (2), the guide-vane turning should be high and the loading low.

An independent analytical analysis concerned with radial (axisymmetric) distortions was conducted in reference 8. In this analysis, it was also recognized that more energy is added by the rotor to the distorted flow region than to the undistorted flow region. As in the analysis of this thesis, an equation was derived for determining the total-pressure difference between the undistorted and distorted flow regions after the flows have passed through the rotor. In reference 8, the undistorted flow is considered to pass through the rotor at a given radius and the distorted flow to follow at the same radius or to pass concurrently at a radius of close proximity whereas in this thesis, the distorted and undistorted flows which are displaced circumferentially are considered to pass concurrently through the rotor at the same radius. The two considerations are different ways of

expressing the same concept and the equations of the two analyses are identities. In reference 8, the equation was plotted and the same conclusions were obtained as in this thesis.

V. EXPERIMENTAL TESTS

In order to check the results of the analysis of the velocity diagrams, a circumferential total-pressure distortion, produced at the entrance of a compressor stage by inserting a 1/4-inch-diameter rod perpendicular to the axis of rotation, was measured upstream and downstream of the rotor.

The velocity diagram analysis considered the flow at a given blade element only, therefore a rotor which has quasi-two-dimensional flow was selected for the tests. The rotor in its original configuration was tested without a guide vane (ref. 9); however, a guide vane is required to produce an included angle of 90° at the entrance to the rotor. Rather than design a guide vane for the rotor, an existing untwisted blade which could be set to produce a 90° included angle at a given radius was used. The mean radius of the rotor was selected for this condition.

Apparatus

A schematic diagram of the 28-inch test compressor is presented in Figure 4. The flow enters from the atmosphere through a honeycomb straightener and three screens. An entrance cone with a contraction ratio of 13:1 is used to accelerate the flow into the test section. The rotor discharges through an annular diffuser. Downstream of the annular diffuser the flow is turned outward through a radial diffuser which can be adjusted to decrease or increase the exit area and thus regulate the

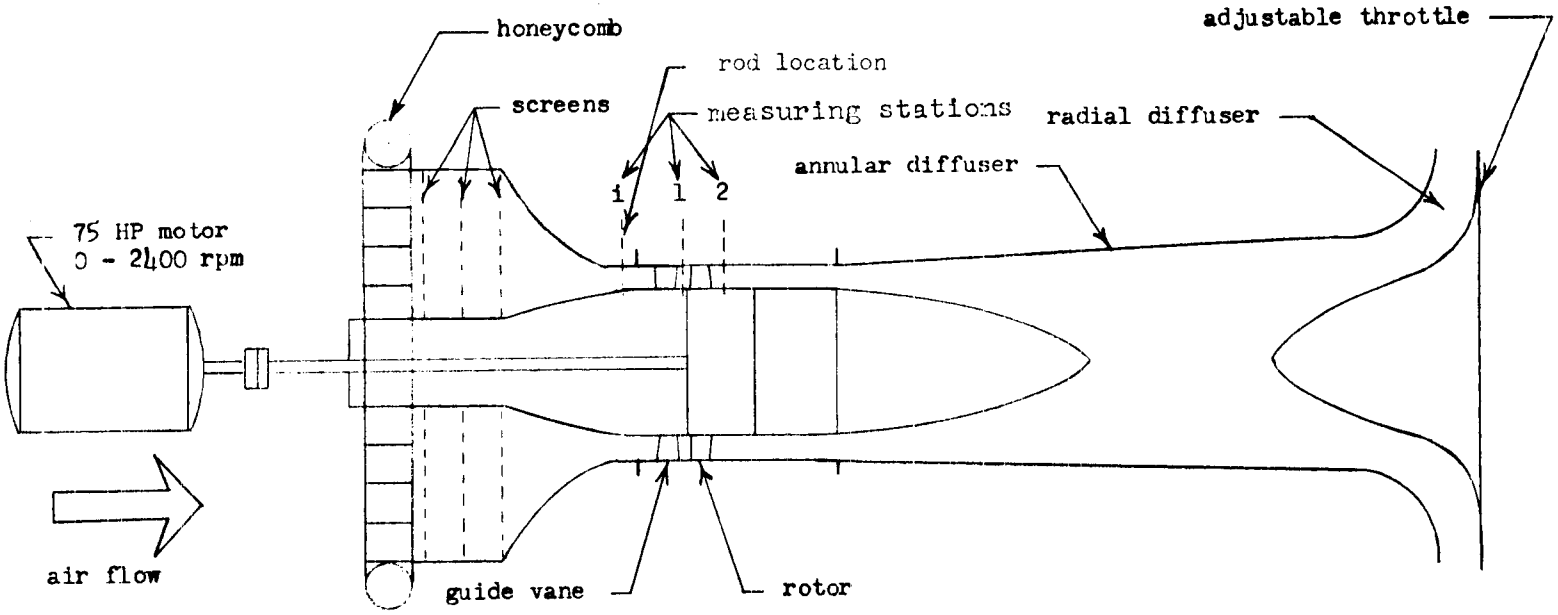

Figure 4.- Schematic diagram of test compressor showing blade rows and instrumentation positions.

flow rate. The drive is a 75-horsepower direct-current motor operable from 0 to 2400 rpm. Figure 5 is a photograph of the rotor used in this investigation. Its performance is given in reference 9. The rotor blades were designed so that the exit tangential velocity was inversely proportional to the radius (free vortex condition) and had medium-camber NACA 65-$(C_{l_o} A_{10})$10 airfoil sections. The following table presents the design details:

Station	NACA Section	α_d, deg	θ_d, deg	$\beta_{1R,d}$ deg	$\beta_{2R,d}$ deg	ξ_d, deg	σ_d	Radius, in.
Hub	65-$(17A_{10})$10	16.0	26.0	48.9	22.9	32.9	1.00	10.91
Mean	65-$(12A_{10})$10	12.5	18.8	52.5	33.7	40.0	1.00	12.41
Tip	65-$(8.5A_{10})$10	10.0	13.8	55.6	41.8	45.6	1.00	13.91

The airfoil sections were formed by combining the NACA 65-010 basic thickness distribution, reference 10, with cambered mean lines. The amount of camber is expressed as the design lift coefficient, c_{l_o}, in tenths for the isolated airfoil. A_{10} indicates that the mean line produces uniform chordwise normal force loading. The blade chord at the mean radius was 3.0 inches. The rotor blades were attached to the hub with threaded blade shanks and lock nuts to allow changes in the blade-setting angle to be made. The guide vane had a constant NACA 65-series airfoil section with zero twist from hub to tip. The

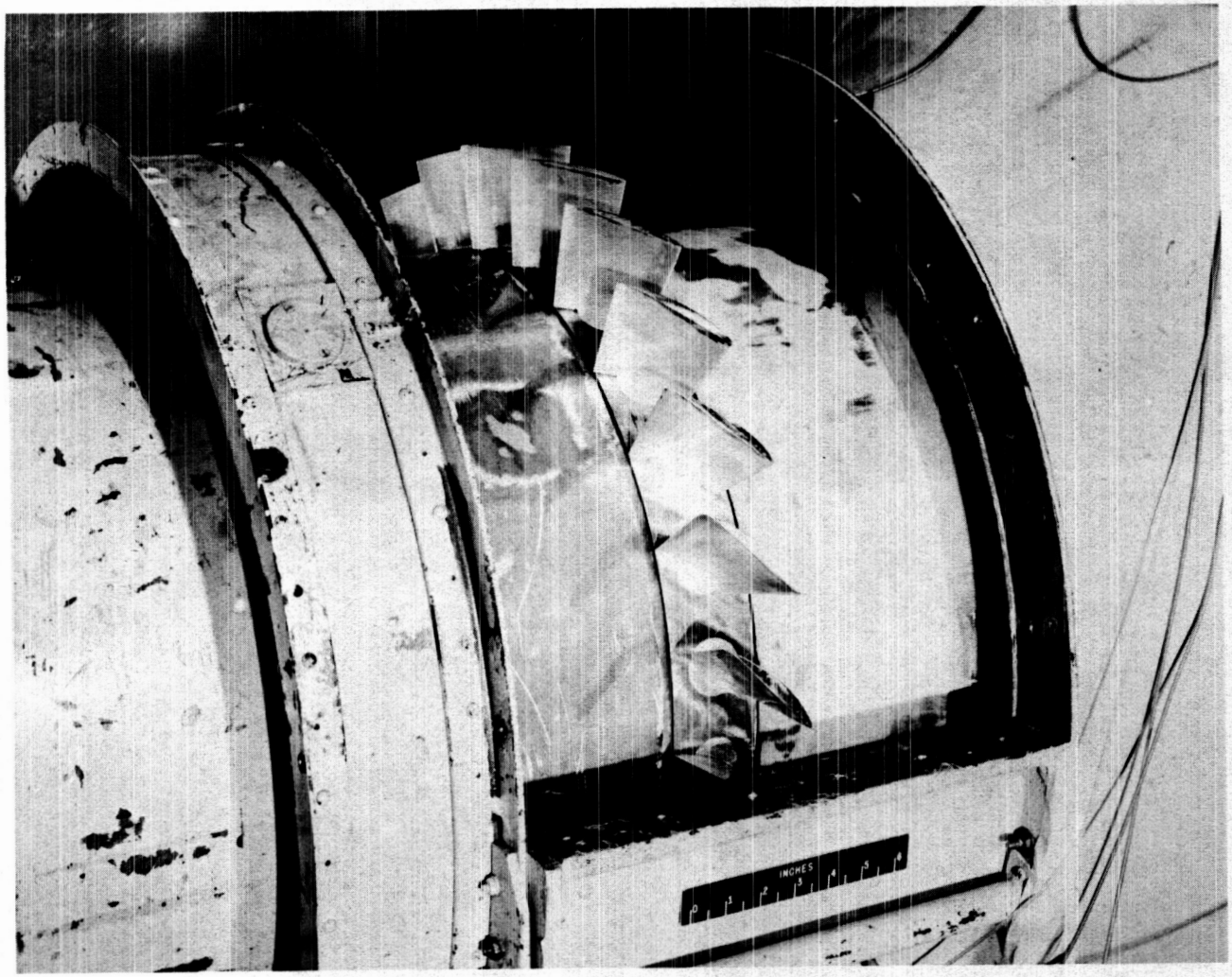

NACA
L-85899

Figure 5.- Rotor used in investigation.

chord and solidity at the mean radius were 2.5 inches and 1.0, respectively. Each blade was attached to the outer casing with a single screw allowing variations in blade-setting angle to be made.

Instrumentation

The measuring stations are shown in Figure 4. Figure 6 shows the instrumentation at each station. The circumferential location of the rod wake upstream of the rotor (station 1) relative to its location at station i depends on the amount and the direction the flow is turned by the guide vanes. The circumferential location of the wake downstream of the rotor (station 2) relative to its location at station i depends not only on its location at station 1 but also on the amount the flow is turned by the rotor which in turn depends on the flow rate. Since the instruments are fixed at the axial and circumferential locations shown in Figure 6 (they are free to move along and rotate about their stem axes only), the rod has to be positioned circumferentially at station i for each flow condition. For this purpose, several rod ports are spaced circumferentially at station i. A prism-type probe capable of sensing static and total pressure and flow direction, Figure 7 and reference 11, was used to determine dynamic pressure at station i. A 26-tube total-pressure rake, Figure 8, was used to measure the rod wake and a prism-type probe was used to measure dynamic pressure and flow direction upstream of the rotor, station 1. A 25-tube shielded total-pressure rake, Figure 9, was used to measure the rod wake

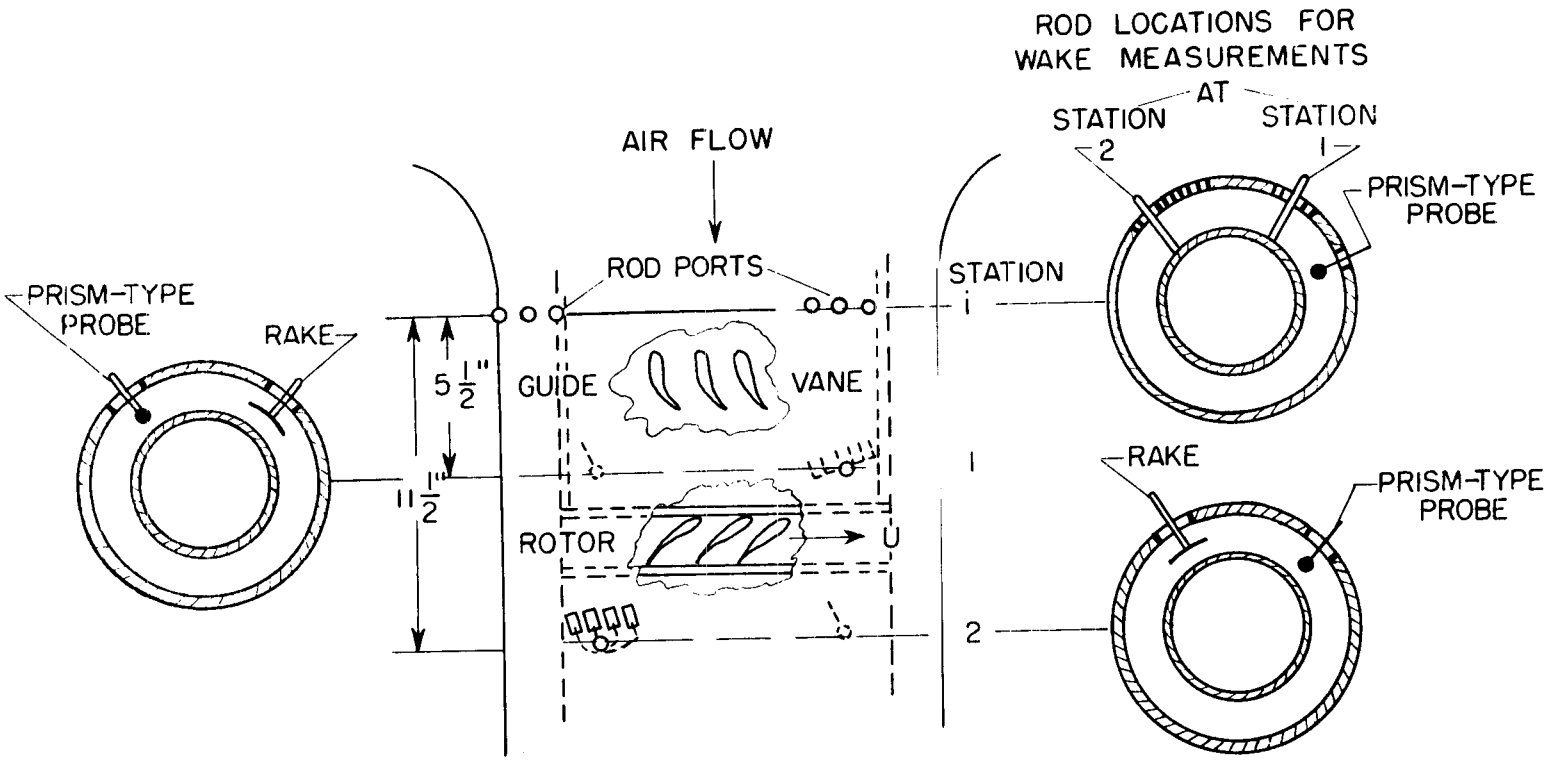

Figure 6.- Sketch showing instrumentation at each measuring station.

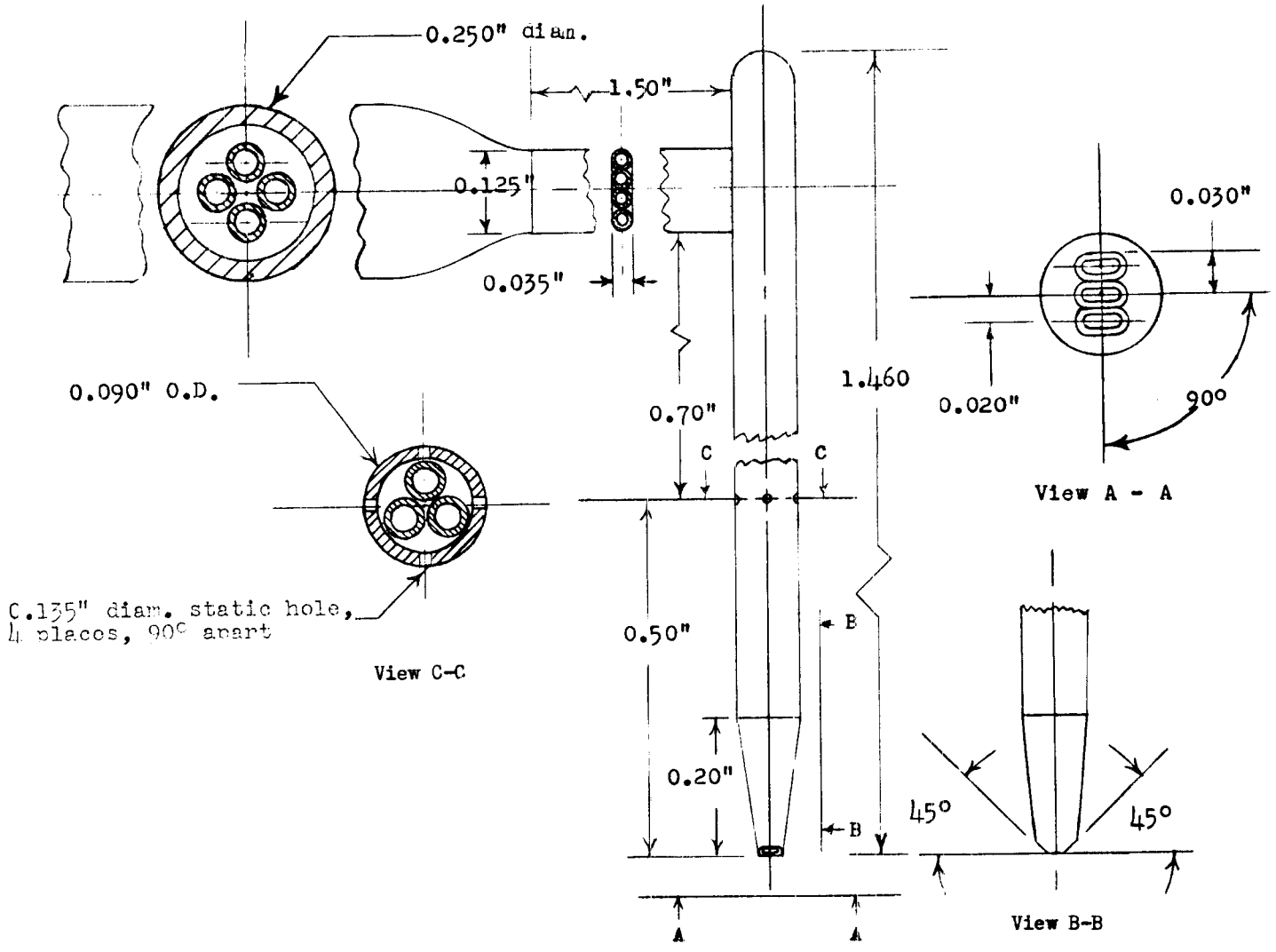

Figure 7.- Details of prism-type probe.

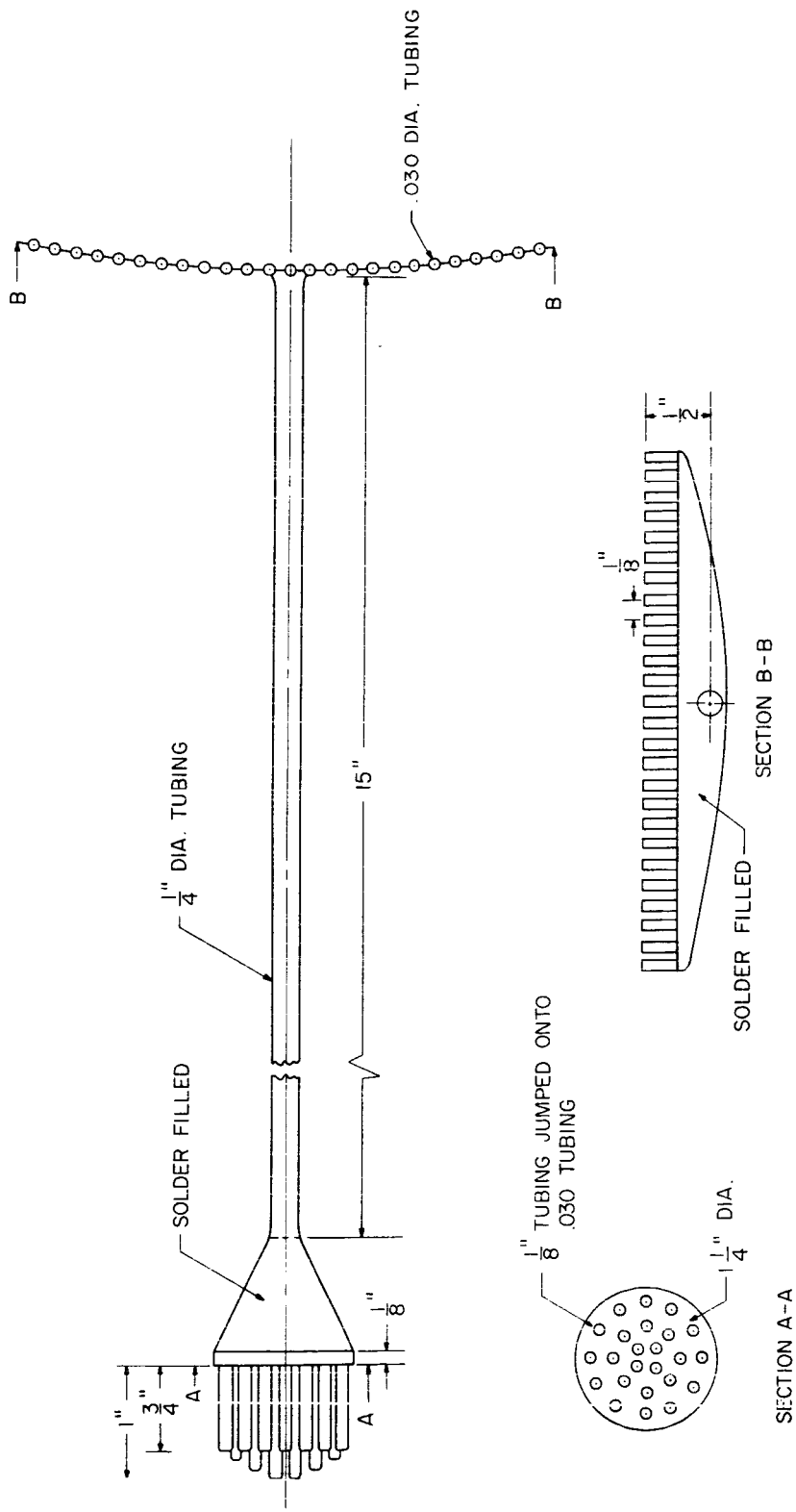

Figure 8.- 26-tube total-pressure rake used to measure rod wake at station 1.

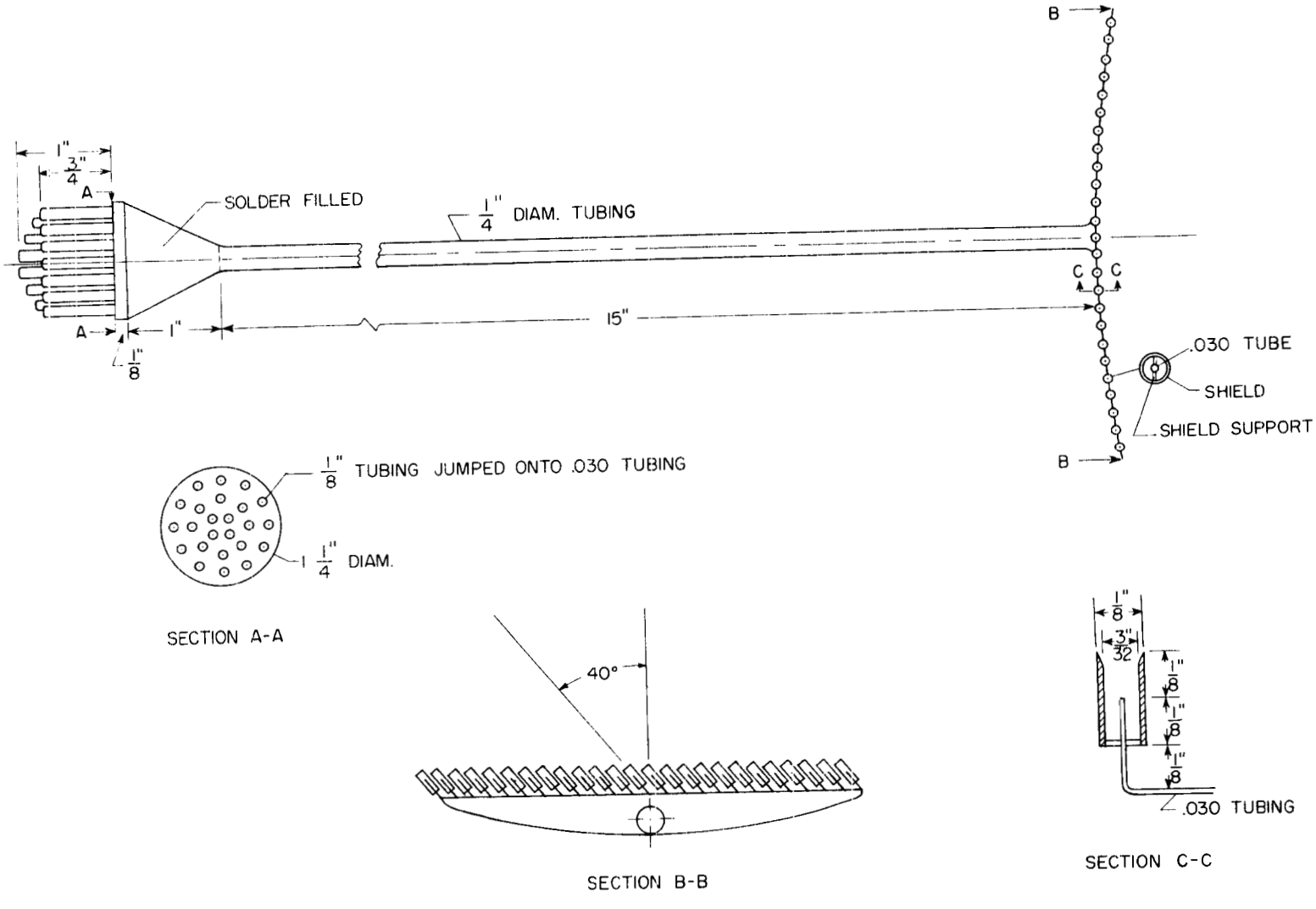

Figure 9.- 25-tube shielded total-pressure rake used to measure rod wake at station 2.

and a prism-type probe was used to measure the dynamic pressure and flow direction downstream of the rotor, station 2. The tubes of the downstream rake were shielded and inclined 40° counterclockwise from the axial direction in order to make the rake insensitive to changes in the exit-flow angle and to provide measurements an equal distance behind the rotor trailing edge. All measurements were made at the mean radius.

Test Program and Procedure

Three rotor-alone and two rotor-guide-vane configurations at a solidity of 1.0 were used to produce various velocity diagrams. For the three rotor-alone configurations the rotor blades were set at design angle of attack when the air inlet angle (β_{1R}) at the mean radius is 45°, 52.5°, and 60°; that is, blade-setting angles at the mean radius of (ξ_d - 7.5°), ξ_d = 40°, and (ξ_d + 7.5°), respectively. For both of the rotor-guide-vane configurations, the rotor blade was set for design angle of attack when the air inlet angle (β_{1R}) is 60° at the mean radius and the guide vane was set to turn the flow 30° in the direction of rotor rotation and also 25° in the opposite direction. Several throttle settings were used for each configuration to provide comparisons at various angles of attack. The rotor speed for all tests was 2,000 rpm. For each test, the rod was first positioned circumferentially so that its wake would pass over the upstream measuring rake (station 1). In order to completely define the wake, pressure

readings were recorded with and without the rod in position. With the instruments at station 1 located close to the outer casing, to prevent interference, the rod was positioned circumferentially so that its wake passed over the downstream measuring rake (station 2) and pressure measurements were recorded with and without the rod in place. In order to insure that the downstream rake measured the complete circumferential extent of the rod wake, measurements were made with the rod in several circumferential locations, approximately 1 inch apart. All pressures were measured by a multiple-tube alcohol manometer board and were recorded simultaneously by photographing the manometers.

The rotor speed was kept within ±5 rpm using a tachometer and a strobotac; the static and total-pressure measurements are considered to be accurate within ±1/2 percent of the dynamic pressure and the measured angles are considered to be accurate within $\pm 1/2^{\circ}$. On the basis of these testing accuracies the wake plots are considered to be correct within ±1.0 percent.

Presentation of Data

All of the wakes are plotted as the ratio of the difference between the total pressure of the undistorted flow and a point in the distorted flow to the dynamic pressure at station i as a function of circumferential distance measured from the center of the wake. Because of mixing losses, the integrated total-pressure deficit between the wake and the undistorted flow would increase as the wake moved downstream. Measurements of the rod wake in a straight duct show that, between

measuring positions corresponding to those in the test (5-1/4 inches and 11-1/4 inches downstream of the rod), the integrated total-pressure deficit would increase by 4.0 percent. Since this change is so small and since the rotor is expected to decrease the integrated total-pressure deficit by 30 to 100 percent, comparisons across the rotor based on $\frac{dP}{q_i}$ will suffice for this thesis. The integrated deficit will differ at the leading edge and at the trailing edge of the blade from those at the upstream and downstream measuring stations, respectively; however, the differences would be less than 4.0 percent and can be considered insignificant.

VI. RESULTS AND DISCUSSION

Figure 10 presents the rod wake measured upstream and downstream of the rotor, together with the downstream wake estimated using equation (2), for the five configurations at approximately design angle of attack. The downstream wakes were measured on the rake with the rod in several circumferential positions. A different symbol is used for each rod position. The test points, both upstream and downstream, are located with respect to the center of the wake. The plots are arranged from the top of the figure in the order of increasing wake elimination, based on the ratio of the area under the estimated downstream curve to the area under the measured upstream curve. The percentages of estimated wake elimination in the order of presentation are 39.3, 39.5, 57.7, 80.5, and 100 (Figures 10(a) to 10(e)), respectively. For all configurations, the measured wakes decrease across the rotor and the percentages of measured wake elimination, in the order presented in Figure 10, are 64.4, 57.0, 77.0, 96.7, and 64.9, respectively. The rotor eliminated a greater portion of the wake than was estimated, with one exception; for the rotor-alone configurations, the trend of increasing wake elimination follows that estimated. The reason for the difference between the estimated and measured percentage of elimination will be explained subsequently. For the rotor-guide-vane configurations (Figures 10(b) and 10(e)), considerable variation between the wakes measured for the several circumferential positions of the rod is evident. Some of the variation may be due to the change of circumferential position of the

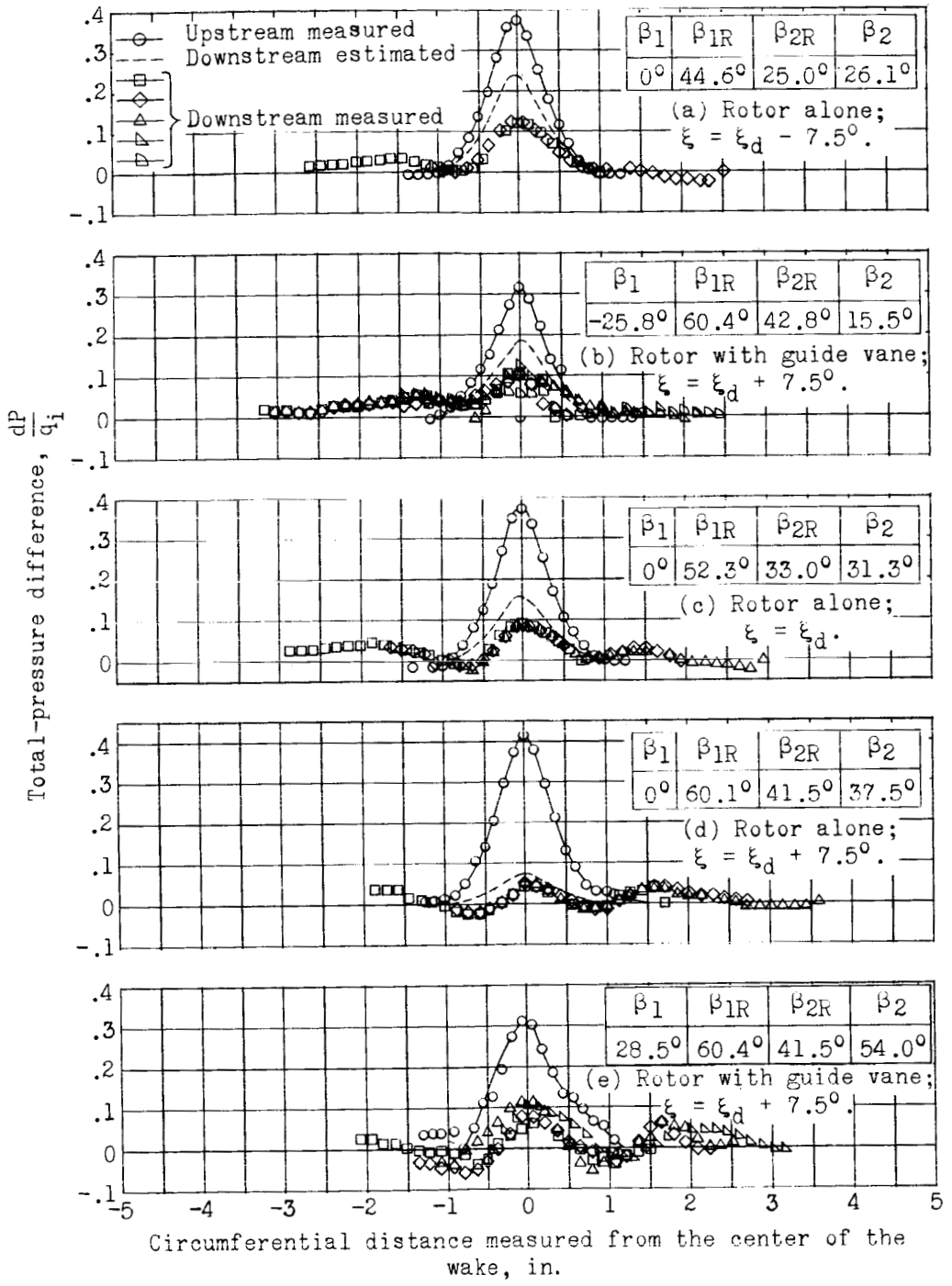

Figure 10.- Comparison of measured and estimated downstream rod wakes with the measured upstream wake for five test configurations at approximately design angle of attack.

rod wake relative to the guide-vane blades. It should be noted that the estimated downstream wakes were calculated for these tests assuming that the streamlines enter and leave the rotor at the same radius, whereas the tests are three dimensional. (Equation (2) applies to three-dimensional flow if the streamline path is known.) The rotor-alone configurations would be closer to two-dimensional flow than the rotor-guide-vane configurations, because the rotor was designed for two-dimensional flow without a guide vane, and the guide vane was not designed for use with this rotor. The mismatching of the rotor and guide vane leads to more pronounced radial flow shifts which alter the shape of the wake across the rotor considerably as manifested in the downstream curves. For the rotor-alone configurations (Figures 10(a), 10(c), and 10(d)), the three-dimensional effects are small, as evidenced at the extremities of the downstream wakes, and the wakes measured at the several circumferential positions coincide.

Figure 11 presents plots for the rotor alone at design blade-setting angle and angles of attack of $\alpha_d - 6.8^\circ$, α_d and $\alpha_d + 7.5^\circ$. The measured wake is reduced across the rotor for all angles of attack and follows the same trend as that estimated with respect to increasing the percentage of wake elimination with increasing angle of attack. The high angle-of-attack plot (Figure 11(c)), shows differences between wake measurements at the various circumferential positions and shape alteration of the wakes across the rotor similar to those of Figure 10(c). Since the radial flow shifts at this angle of attack are more pronounced than at design angle of attack, Figure 11(c) provides more evidence that

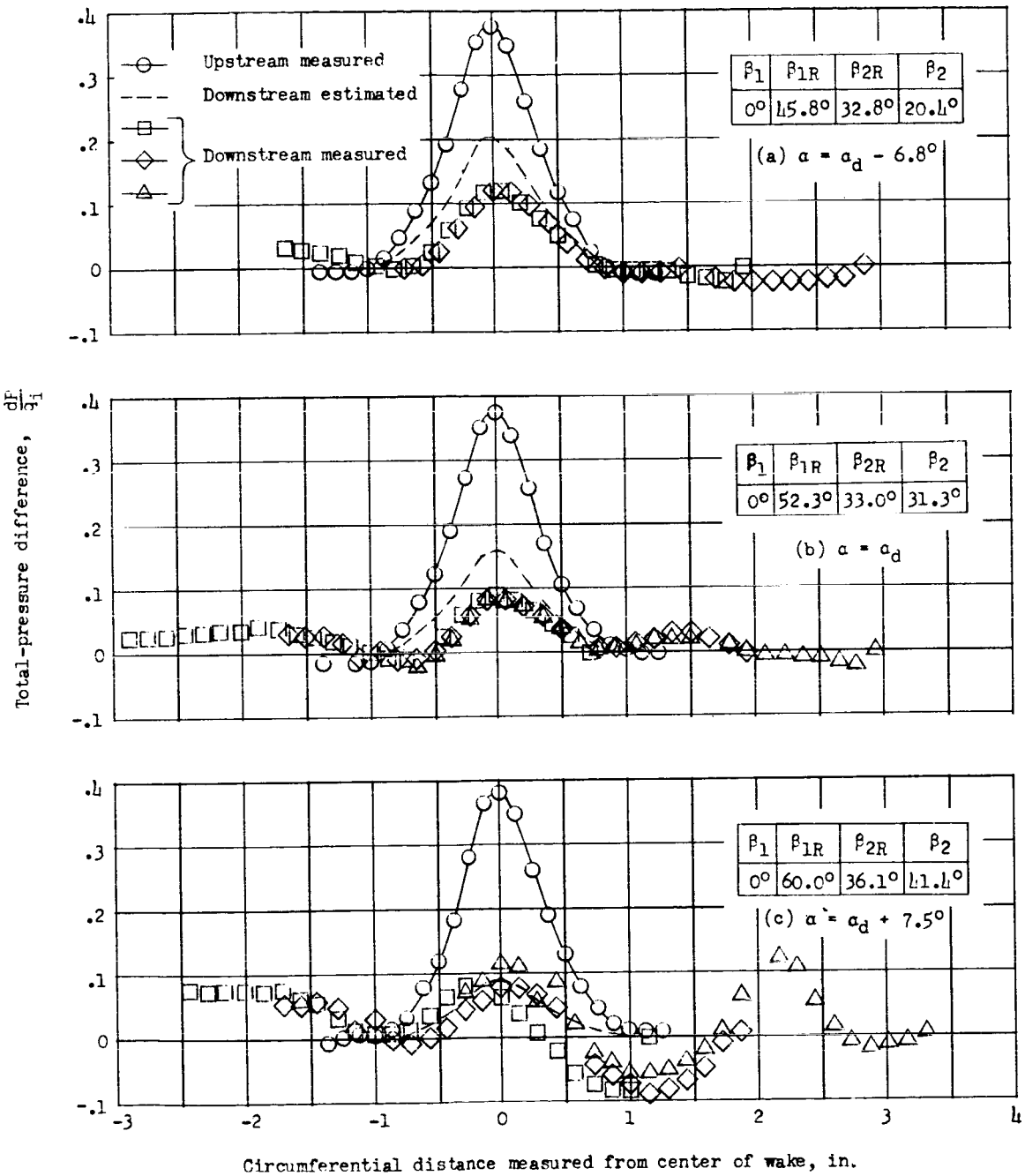

Figure 11.- Comparison of measured and estimated downstream rod wakes with measured upstream wake for rotor alone; $\xi = \xi_d$, configuration at three angles of attack.

the difference between the wakes measured at the several circumferential positions and the shape alteration of the wake across the rotor in Figure 10(e) are a result of radial flow shifts.

Considering the rotor-alone plots (since they are closer to two-dimensional flow) in Figures 10 and 11, it is noted that, since the measured wake elimination follows the estimated trend, the experimental results verify the conclusion of the theoretical analysis; that is, the degree of distortion elimination is a function of the magnitude of the angles of the velocity diagram. Contrary to the prediction of the velocity-diagram analysis, the velocity diagram with one included angle approximately 90° and the other slightly larger than 90° failed to eliminate the distortion completely because of three-dimensional effects; however, the three rotor-alone tests of Figure 10 provide some proof that a 90° included angle may be optimum for eliminating a distortion across a stage. For these three velocity diagrams, the value of the bracketed term of equation (2), excluding the exit included-angle term, $\cos(\beta_2 + \beta_{2R})$, had values of 1.01, 0.98, and 0.94 for Figures 10(a), 10(c), and 10(d), respectively. These values represent the ratio of the integrated estimated downstream wake to the integrated upstream wake. The percentages of wake elimination for the three diagrams are therefore -1.0 percent, 2.0 percent, and 6.0 percent. The differences between the three configurations are small, whereas the estimated values, including the exit included-angle term, are 39.3 percent, 57.7 percent, and 80.5 percent. The larger differences between the three configurations indicate that the predominant term is the exit included angle. The measured

percentages of wake elimination for the three diagrams, 64.4, 77.0, and 96.7 for exit included angles of 51.1°, 64.3°, and 79.0°, respectively, have differences between them of the same order as those between the estimated values; therefore, the advantage of the exit included angle approaching 90° is evident.

As noted previously, the measured wake was reduced a greater amount than that estimated; therefore, the wake was energized to a greater extent than calculated. A reappraisal of the initial assumptions upon which equation (2) was based shows that, in order to produce a greater work input than estimated, either a greater diffusion occurs in the wake ($p_2$distortion > p_2) or the low-energy air experiences a greater turning than that assumed $\frac{d\theta}{d\alpha} > 1.0$. The existence of a difference between the static pressure in a wake and in the surrounding flow is contrary to experience; therefore, the low-energy air must have been overturned. Since the rotor is subjected to the angles of attack in the wake for a short period of time, the static-pressure field in the blade passage is dictated by the undistorted flow. The centrifugal force arising from the turning of the flow in the blade passage is related to the pressure gradient normal to the direction of the streamline by

$$\frac{dp}{dr} = \rho \frac{V_p^2}{r}$$

where r is the radius of curvature of the streamline. Therefore, because the relative velocity of the wake particles is lower than that of the undistorted flow, the wake particles will not be in equilibrium with the surrounding pressure field unless the radius of curvature of the

streamline is smaller at all points, Figure 12. The net result is an overturning of the distorted flow.

There are indications that this overturning is true. As blade-setting angle or undistorted-flow angle of attack increases, the difference between the relative velocities of the two flows becomes smaller and less difference in the radius of curvature of the streamline is required to maintain equilibrium. As blade-setting angle (Figure 10) and angle of attack (Figure 11) increases, the measured wake is more nearly equal to that estimated. At this point, it should be noted that equation (2) would estimate the downstream wake more accurately for inlet flow distortions which are of large enough circumferential extent to alter the static-pressure field in the blade passage if the angle of attack in the distorted flow is not large enough to cause blade stall.

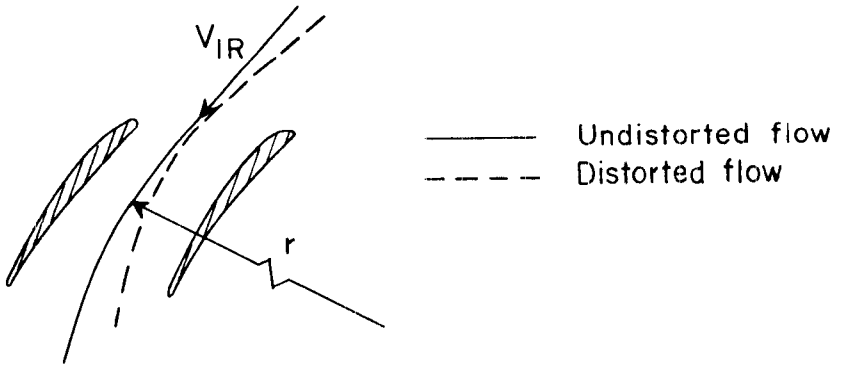

Figure 12.- Comparison of the streamline paths of the undistorted and distorted flows in the blade passage.

VII. CONCLUSIONS

A preliminary theoretical and experimental investigation of the effect of velocity diagram parameters on inlet total-pressure distortions through a single-stage subsonic axial-flow compressor for incompressible flow has been conducted. The wake of a 1/4-inch-diameter rod, measured both upstream and downstream of a rotor, has been compared for various velocity diagrams. The measured downstream wake was also compared with the downstream wake estimated by using a derived equation subject to the assumptions that (a) the undistorted and distorted flows enter the rotor with the same absolute direction, (b) the static pressures of the undistorted and distorted flows are equal at the inlet and also at the exit of the rotor, (c) the increase of blade angle of attack in the distorted flow is not sufficient to cause blade stall, and (d) the distorted flow is turned in the rotor passage to the same exit direction, relative to the rotor, as the undistorted flow. As a result of this investigation, the following conclusions are made:

1. Velocity diagrams for which the included angle between the relative and absolute flow directions is 90°, at either the inlet or exit of the rotor, are indicated to be optimum for eliminating inlet total-pressure distortions across the first stage of a compressor. A flow coefficient of 0.5 or less is required, but loading (turning angle) has no apparent influence.

2. Velocity diagrams, with one of the included angles greater than 90°, will increase the total pressure of the distortion beyond that of

the undistorted total pressure. However, if both included angles are greater than 90°, the inlet total-pressure distortion will not be completely eliminated. For these results, either or both the entering and exiting flow coefficients must be less than 0.5.

3. When the velocity diagram has neither of the included angles equal to 90°, the decrease in the inlet total-pressure distortion across the rotor depends not only on the magnitude of the inlet and exit included angles, but also on the relative magnitude of the absolute and relative flow angles at the inlet and at the exit. Both flow coefficient and loading influence the amount of distortion elimination. The flow coefficient should not be too much greater than 0.5, the guide-vane exiting angle should be high, and the loading should be low for the greatest elimination of distortion by the rotor.

4. The experimental tests show that the derived equation will estimate the downstream distortion with reasonable accuracy for inlet total-pressure distortions which extend far enough circumferentially to alter the static-pressure field in the blade passage.

The purpose of the velocity diagram analysis given in the thesis was to determine the velocity diagram which would be most effective in reducing an inlet total-pressure distortion. This has been accomplished under the given assumptions. However, the analysis of a velocity diagram at a single blade element does not give a complete picture of the flow through a compressor stage. The mutual effects of the flow at all radial stations depend on the particular design of the compressor stage

and are numerous and complex when the flow is undistorted. Therefore, it appears that the accomplishment of a complete criterion for designing compressor stages which will eliminate an inlet total-pressure distortion will develop primarily from experimental tests. Future experimentation should include tests of compressor stages having included angles of 90° at all blade elements and tests where the flow is compressible. Reference 8 provides a compressible flow equation for determining the amount of distortion elimination at a given blade element.

VIII. SUMMARY

A preliminary theoretical and experimental investigation of the effect of velocity diagram parameters on inlet total-pressure distortions through single stage subsonic axial-flow compressors for incompressible flow has been conducted. As a result of the theoretical investigation, velocity diagrams with an included angle of 90° between the absolute and relative flow directions either at the inlet or exit (with flow coefficient not greater than 0.5) were indicated to be optimum for elimination of total-pressure distortion by a single compressor stage. When an included angle is 90°, loading (turning angle) has no apparent influence; however, for included angles less than 90°, the loading should be low.

For the experimental tests, the wake of a 1/4-inch-diameter rod was measured upstream of the rotor. By using the measured upstream wake and a derived equation for incompressible flow, the wake downstream of the rotor was estimated and compared with the measured downstream wake for several velocity diagrams.

The rod wakes of the experimental tests were of such small circumferential extent that the undistorted flow dictated the static-pressure field in the blade passage. Flow equilibrium with this pressure field required a smaller radius of curvature of the streamline for the distorted flow and resulted in greater turning and therefore, a greater energy addition than that estimated. However, for inlet total-pressure distortions which extend far enough circumferentially to alter the

static-pressure field in the blade passage, the derived equation will estimate the downstream distortion with reasonable accuracy.

IX. ACKNOWLEDGMENTS

The author wishes to express his appreciation to the National Advisory Committee for Aeronautics for the opportunity to use material in this thesis which was obtained from a research project conducted at the Langley Laboratory.

[redacted]

X. BIBLIOGRAPHY

1. Sterbentz, William H.: Factors Controlling Air-Inlet Flow Distortions. NACA RM E56A30, 1956.

2. Walker, Curtis L., Sivo, Joseph N., and Jansen, Emmert T.: Effects of Unequal Air-Flow Distribution From Twin Inlet Ducts on Performance of an Axial-Flow Turbojet Engine. NACA RM E54E13, 1954.

3. Penn, David B., and Sivo, Joseph N.: Effect of Inlet Flow Distortion on Compressor Stall and Acceleration Characteristics of a J65-B-3 Turbojet Engine. NACA RM E55F20, 1955.

4. Piercy, Thomas G., and Klann, John L.: Experimental Investigation of Methods of Improving Diffuser-Exit Total-Pressure Profiles for a Side-Inlet Model at Mach Number 3.05. NACA RM E55F24, 1955.

5. Smith, Ivan D., Braithewaite, W. M., and Calvert, Howard F.: Effect of Inlet-Air-Flow Distortions on Steady-State Performance of J65-B-3 Turbojet Engine. NACA RM E55I09, 1956.

6. Conrad, E. William, and Sobolewski, Adam E.: Investigation of Effects of Inlet-Air Velocity Distortion on Performance of Turbojet Engine. NACA RM E50G11.

7. Steffens, C., Jr., Throndson, L. W., and Kapplin, C. H.: Development of a Method for Correlating the Effect of Various Types of Circumferential Inflow Distortion on the Stall Characteristics of Axial-Flow Compressor Engines. Pratt and Whitney Report No. PWA Inst. 480, Sept. 1955.

8. Smith, L. H., Jr.: Recovery Ratio - A Measure of the Loss Recovery Potential of Compressor Stages. Paper No. 56-A-206, A.S.M.E. (Presented at A.S.M.E. Annual Meeting, New York, Nov. 25-30, 1956.)

9. Ashby, George C., Jr.: Comparison of Low-Speed Rotor and Cascade Performance for Medium-Camber NACA 65-(C_{l_o} A_{10})10 Compressor-Blade Sections Over a Wide Range of Rotor Blade-Setting Angles at Solidities of 1.0 and 0.5. NACA RM L54I13, 1954.

10. Abbott, Ira H., Von Doenhoff, Albert E., and Stivers, Louis S., Jr.: Summary of Airfoil Data. NACA Rep. 824, 1945. (Supersedes NACA WR-560.)

11. Schulze, Wallace M., Ashby, George C., Jr., and Erwin, John R.: Several Combination Probes for Surveying Static and Total Pressure and Flow Direction. NACA TN 2830, 1952.

XI. VITA

The author was born in Smithfield, Virginia on October 15, 1925. He graduated from the Newport News High School in Newport News, Virginia in 1943. After service in the Army Air Force during World War II, he received the Degree of Bachelor of Science in Aeronautical Engineering from the Virginia Polytechnic Institute in June 1950. Since that time he has been employed as an Aeronautical Research Engineer by the National Advisory Committee for Aeronautics at Langley Field, Virginia.

George C. Ashby, Jr.

XII. APPENDIX

DETERMINATION OF THE EQUATION FOR ESTIMATING THE TOTAL-PRESSURE DIFFERENCE BETWEEN THE UNDISTORTED FLOW AND A POINT IN THE DISTORTED FLOW AFTER THE FLOW HAS PASSED THROUGH THE ROTOR

The equation for the energy added by the rotor is

$$H_2 - H_1 = U_2 V_{t,2} - U_1 V_{t,1} \tag{A1}$$

Since $H = u + \frac{p}{\rho}$ the energy added by the rotor can also be expressed as

$$H_2 - H_1 = u_2 - u_1 + \frac{p_2}{\rho_2} - \frac{p_1}{\rho_1} \tag{A2}$$

By definition $u = c_v t$ or using the perfect gas law ($p = \rho R t$)

$$u = \frac{c_v p}{\rho R}$$

Substituting in (A2) and assuming incompressible flow, (A2) becomes

$$H_2 - H_1 = \frac{c_v}{R\rho}\left(p_2 - p_1\right) + \frac{p_2 - p_1}{\rho} \tag{A3}$$

Equating (A1) and (A3) and rearranging gives

$$\frac{p_2}{\rho} = \frac{p_1}{\rho} + U_2 V_{t,2} - U_1 V_{t,1} - \frac{c_v}{R\rho}\left(p_2 - p_1\right) \tag{A4}$$

The total-pressure difference between the undistorted flow and a point in the distorted flow entering the rotor is a function of the difference in the squares of the absolute velocities; therefore, the variation in total pressure between the two flow regions downstream of the rotor will be determined with respect to $V_1^2/2$.

Since U_2 and U_1 are constant for a given velocity diagram, c_v and R are constants, ρ is constant for incompressible flow and $(p_2 - p_1)$ is constant under assumption 2 of "ANALYSIS," $\frac{p_2}{\rho}$, $\frac{p_1}{\rho}$, $V_{t,1}$ and $V_{t,2}$ are the only variables with respect to $V_1^2/2$ in equation (A4). It can be seen from Figure 3(b) that

$$V_{t,1} = V_1 \sin \beta_1 = \sqrt{2}\sqrt{V_1^2/2} \sin \beta_1 \tag{A5}$$

$$V_{t,2} = U_2 - V_{t,2R} = U_2 - V_{2R} \sin \beta_{2R} \tag{A6a}$$

Under assumptions 1 and 4 of "ANALYSIS" $\sin \beta_1$ and $\sin \beta_{1R}$ are constants with respect to $V_1^2/2$; therefore, the velocity V_{2R} is the only remaining variable. The velocity V_{2R}, in terms of $V_1^2/2$, can be obtained from the relative enthalpy rise which is

$$H_{2R} - H_{1R} = \frac{U_2^2 - U_1^2}{2} = \frac{c_p}{R\rho}(p_2 - p_1) + \frac{V_{2R}^2}{2} - \frac{V_{1R}^2}{2} \tag{A6b}$$

From Figure 3(b) it can be seen that

$$V_{1R}^2 = V_{a1}^2 + V_{t,1R}^2 = V_{a1}^2 + (U_1 - V_{t,1})^2 = V_{a1}^2 + U_1^2 - 2UV_{t,1} + V_{t,1}^2$$

Substituting $V_1^2 = V_{a1}^2 + V_{t,1}^2$ and using equation (A5) we obtain

$$V_{1R}^2 = U_1^2 - 2U_1\sqrt{2}\sqrt{V_1^2/2}\sin\beta_1 + 2\left(V_1^2/2\right) \qquad (A6c)$$

Then, substituting equation (A6c) into equation (A6b) and rearranging, the velocity V_{2R} in terms of $V_1^2/2$ is as follows:

$$V_{2R} = \sqrt{U_2^2 - 2U_1\sqrt{2}\sqrt{V_1^2/2}\sin\beta_1 + 2\left(V_1^2/2\right) - \frac{2c_p}{R\rho}\left(p_2 - p_1\right)} \qquad (A6d)$$

Substituting equation (A6d) into equation (A6a) results in

$$V_{t,2} = U_2 - \sin\beta_{2R}\sqrt{U_2^2 - 2U_1\sqrt{2}\sqrt{V_1^2/2}\sin\beta_1 + 2\left(V_1^2/2\right) - \frac{2c_p}{R\rho}\left(p_2 - p_1\right)} \qquad (A6e)$$

Combining equations (A4), (A5) and (A6e) gives

$$\frac{p_2}{\rho} = \frac{p_1}{\rho} + U_2^2 - U_2\sin\beta_{2R}\sqrt{U_2^2 - 2U_1\sqrt{2}\sqrt{V_1^2/2}\sin\beta_1 + 2\left(V_1^2/2\right) - \frac{2c_p}{R\rho}\left(p_2 - p_1\right)} - U_1\sqrt{2}\sqrt{V_1^2/2}\sin\beta_1 - \frac{c_v}{R\rho}\left(p_2 - p_1\right) \qquad (A7)$$

Taking the derivative of equation (A7) with respect to $V_1^2/2$ results in

$$\frac{dp_2}{d\left(V_1^2/2\right)} = \frac{dp_1}{d\left(V_1^2/2\right)} + \rho\left[\frac{\left(U_2\sin\beta_{2R}\right)\left(U_1\sin\beta_1\right)}{V_{2R}V_1} - \frac{U_2\sin\beta_{2R}}{V_{2R}} - \frac{U_1\sin\beta_1}{V_1}\right] \qquad (A8)$$

Multiplying both sides of equation (A8) by $d\left(V_1^2/2\right)$ and substituting $\rho\, d\left(V_1^2/2\right) = dq_1 = dP_1$ gives

$$dP_2 = dP_1\left[1 + \frac{(U_2 \sin \beta_{2R})(U_1 \sin \beta_1)}{V_{2R}V_1} - \frac{U_2 \sin \beta_{2R}}{V_{2R}} - \frac{U_1 \sin \beta_1}{V_1}\right] \quad (A9)$$

Multiplying the appropriate terms by $\frac{V_{a1}}{V_{a1}}$ or $\frac{V_{a2}}{V_{a2}}$ and substituting $\cos \beta = \frac{V_a}{V}$ and $\cos \beta_R = \frac{V_a}{V_R}$ results in the following equation:

$$dP_2 = dP_1\left[1 + \left(\frac{U_2}{V_{a2}} \cos \beta_{2R} \sin \beta_{2R}\right)\left(\frac{U_1}{V_{a1}} \cos \beta_1 \sin \beta_1\right) - \frac{U_2}{V_{a2}} \cos \beta_{2R} \sin \beta_{2R} - \frac{U_1}{V_{a1}} \cos \beta_1 \sin \beta_1\right] \quad (A10)$$

Substituting $\frac{U}{V_a} = \frac{\sin \beta}{\cos \beta} + \frac{\sin \beta_R}{\cos \beta_R}$ in equation (A10), using the identity $\cos\left(\beta + \beta_R\right) = \cos \beta \cos \beta_R - \sin \beta \sin \beta_R$, and rearranging gives

$$dP_2 = dP_1\left[\cos\left(\beta_1 + \beta_{1R}\right) \cos\left(\beta_2 + \beta_{2R}\right) \frac{\cos \beta_1}{\cos \beta_{1R}} \frac{\cos \beta_{2R}}{\cos \beta_2}\right] \quad (A11)$$

This is the equation for the total-pressure deficit between any point in the undistorted flow region and a point in the distorted flow after the flow has passed through the rotor. If the upstream total-pressure deficit and the velocity diagram for the undistorted flow is known, the downstream total-pressure deficit can be obtained.